Journal of Science and Technology in Civil Engineering, HUCE (NUCE), 2022, 16 (3): 152–165

ASSESSING THE SHEAR BEHAVIOR OF CORRODED STEEL FIBER REINFORCED CONCRETE BEAMS WITHOUT SHEAR REINFORCEMENT USING NONLINEAR FINITE ELEMENT ANALYSIS

Nguyen Ngoc Tan[a,*], Nguyen Thi Thanh Thao[a], Nguyen Tien Van[a], Du Duc Hieu[a]

[a]*Faculty of Building and Industrial Construction, Hanoi University of Civil Engineering, 55 Giai Phong road, Hai Ba Trung district, Hanoi, Vietnam*

Article history:
Received 04/5/2022, Revised 24/6/2022, Accepted 27/6/2022

Abstract

The shear behavior of steel fiber reinforced concrete (SFRC) beams has been assessed in a large number of previous studies. However, the shear strength of corroded SFRC beams without shear reinforcement is still an unresolved topic. In this paper, the finite element models of non-corroded and corroded SFRC beams have been constructed and verified regarding load-displacement curves, crack patterns, and failure modes. Finally, a parametric study also was performed to assess the effect of essential design parameters on the shear strength of SFRC beams under corrosion attacks. The results show that the reinforcement corrosion degree and concrete compressive strength are the most influencing parameters on the shear strength of SFRC beams, followed by the shear span-to-depth ratio and the steel-reinforced ratio.

Keywords: shear strength; steel fiber reinforced concrete (SFRC); steel corrosion; nonlinear finite element analysis.

https://doi.org/10.31814/stce.huce(nuce)2022-16(3)-12

1. Introduction

Steel corrosion is one of the leading causes of the degradation of reinforced concrete (RC) structures. Steel corrosion induces cross-section loss, crack propagation, and bond strength loss in RC members [1–4]. An average decrease of about 20% in both flexural strength and shear strength in corroded structures was reported by Soltani et al. [2]. Estimating the shear strength is important in the design of civil engineering projects because of the unexpected brittle behavior of RC beams, especially corroded RC beams [5]. Therefore, many researchers undertook experimental, analytical, and empirical studies to determine the shear capacity of corroded RC beams [6–11].

Additionally, the bond strength enables reinforcement to be subjected to the same strain as the surrounding concrete [12]. That is why bond strength loss is one of the primary impacts of corrosion when deteriorating RC structures occur. There are numerous experimental studies conducted in this field. For example, Kim et al. [13] observed that the bond action accounts for 25-30% of the overall shear force. According to the numerical models conducted by Nguyen et al. [11], corroded beams with a 90% bond loss have a maximum loading capacity of decreasing to roughly 50%.

*Corresponding author. *E-mail address:* tannn@huce.edu.vn (Tan, N. N.)

On the other hand, with its advantages, steel fiber reinforced concrete (SFRC) has been used widely worldwide in building construction. SFRC increases the mechanical properties of ordinary concrete, especially tensile strength and post-crack strength [14–17]. Therefore, steel fiber in concrete could act as a barrier to the propagation of corrosion cracks due to the restricted migration and diffusion transport capabilities. However, this characteristic of SFRC is rarely discussed.

Currently, numerous studies are being conducted to propose the prediction models for the shear strength of SFRC beams [18, 19]. However, until now, no model has been developed to predict the shear strength of corroded SFRC structures. Besides, Taqi et al. [20] investigated the effect of steel corrosion for longitudinal reinforcement on the shear behavior of SFRC beams with and without pre-corroded steel fibers in a concrete matrix. This experimental study concluded that when steel fibers were added, ranging from 0.8% to 1.8% in volume fractions, the shear strength of corroded SFRC beams with or without corroded steel fiber was less than that of non-corroded beams, although adding 1.8% steel fibers improved the shear strength of both non-corroded and corroded beams.

As a result, this study will concentrate on the shear strength of corroded SFRC beams. First, the modeled beams were built and validated using the beam specimens tested in the experimental study of Taqi et al. [20]. Then, after conducting a good validation for nonlinear finite element (NLFE) models for SFRC beams, a series of modeled beams was extended in a parametric study to assess the effect of critical design-oriented parameters on shear behavior (i.e., the concrete compressive strength, the bond strength loss, the corrosion degree, and the shear span-to-effective depth ratio).

2. Presentation of beam specimens

This section presents two beam specimens with dimensions of 100 × 150 × 1300 mm that were tested in the experimental study conducted by Taqi et al. [20]. These beams have been used to simulate the shear behavior using the NLFE method based on the experimental results (e.g., the load-displacement curves, failure mode, and crack pattern). The non-corroded SFRC beam was named BF-1.2 as the control beam, while the corroded SFRC beam was named BC-1.2-7, as shown in Fig. 1. For the corroded SFRC beam, the corrosion degree was approximately 7% based on the mass loss of longitudinal steel rebars. These beams were made of SFRC, having a 1.2% steel fiber content by volume, corresponding to 84 kg/m^3 in the mixture. The concrete compressive strength is 43 MPa, which was measured on cylindrical samples with a 150 mm diameter and a 300 mm height at 28 days. The steel fibers used are typed hook-end, with a length-to-diameter ratio of 55.6 corresponding to 50 and 0.9 mm in length and diameter, respectively. These hooked-end fibers are steel with a tensile strength of 1150 MPa. It is noted that the steel fibers used were not corroded at the time of casting. As shown in Fig. 1, only tensile longitudinal steel rebars at the bottom layer with a nominal diameter of 10 mm were used to reinforce the beam specimens. In order to induce shear failure, these two

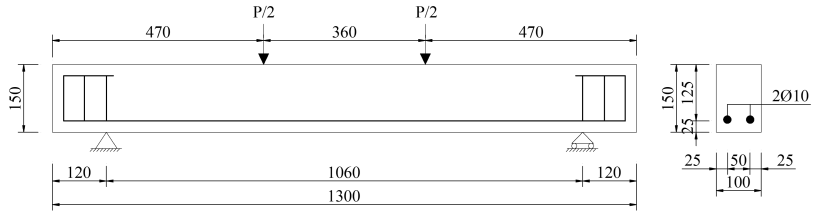

Figure 1. Detailed layout of beam specimens [20]

steel rebars were anchored with 90-degree hooks, and four stirrups with a nominal diameter of 8 mm were placed outside the supports at both ends of the beam. The results obtained from the tension test showed that the yield and ultimate tensile strengths are 560 and 652 MPa for longitudinal rebars and 534 and 757 MPa for stirrups.

3. Finite element modeling of SFRC beams

3.1. Steel fiber reinforced concrete modeling

The material behavior of concrete in DIANA FEA could be modeled based on total-strain crack models (i.e., smeared crack model) [21]. In this case, it is recommended to use the crack bandwidth (h) for defining the smeared length in the finite element model, where h can be estimated as the cubic root of the element's volume (V). The previous study also presents that adding steel fibers with different contents could not affect the SFRC compressive strength [16]. As a result, the constitutive model of concrete in compression is utilized to describe and predict the behavior of corroded SFRC in compression.

Fig. 2(a) depicts the stress-strain relationship of SFRC in compression in non-corroded and corroded conditions in FEM. These stress-strain curves show that the linear-elastic stress of non-corroded concrete is considered when it is less than 30% of the compressive strength. Corrosion products induced a reduction in compressive strength of damaged zones. Compressive fracture energy (G_c) is used to determine the maximum compressive strain required to induce crushing damage in ordinary concrete [22, 23]. Since the compressive strength of SFRC is insignificantly affected by steel fiber content, the behavior of concrete in compression is characterized by a parabolic curve similar to that of ordinary concrete.

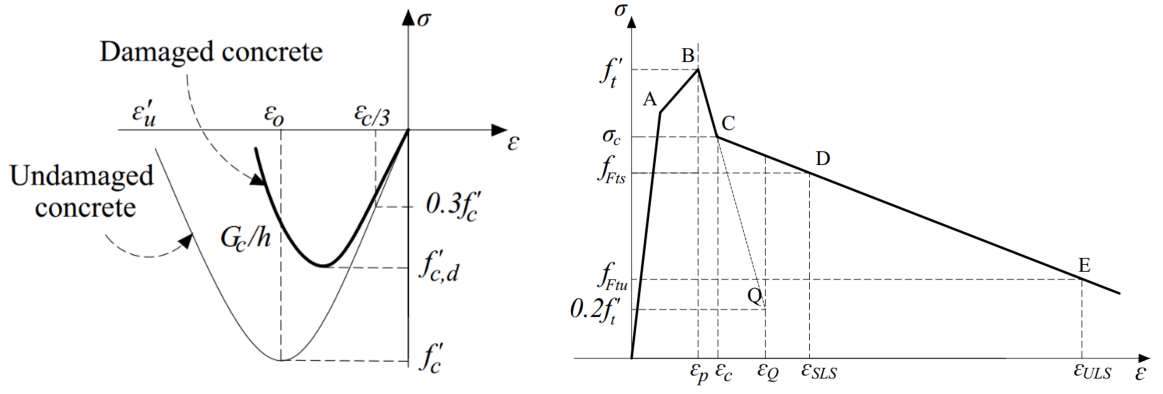

(a) Concrete in compression (b) Concrete in tension

Figure 2. SFRC constitutive model

Eq. (1) calculates the concrete compressive strength in the damaged zone ($f'_{c,d}$) due to steel reinforcement corrosion. In which ε_0 is the compressive strain corresponding to the concrete compressive strength; ε_1 is the average smeared tensile strain, which is computed by Eq. (2); k' is the ratio related to the roughness and diameter of steel rebars. This study sets k' as 0.1 as proposed by Cape [24].

$$f'_{c,d} = f'_c / \left[1 + k' \left(\varepsilon_1 / \varepsilon_0\right)\right] \tag{1}$$

$$\varepsilon_1 = \left(b_f - b_0\right)/b_0 \tag{2}$$

$$b_f - b_0 = n_{bars} w_{cr} \text{ with } w_{cr} = 2\left(v_{rs} - 1\right) X_d \text{ and } X_d = 0.0116 i_{corr} t \tag{3}$$

where: b_0 is the beamwidth with no crack; b_f is the beam width considering corrosion cracks. The modification in section width is calculated by Eq. (3) according to the number of rebars (n_{bars}) and the total crack width (w_{cr}). The total crack width could be calculated from the experimental data or model proposed by Molina et al. [25]. This model considers the ratio between the volume of rust and initial rebar (v_{rs}) and the depth of corrosion crack (X_d). In the present study, v_{rs} is taken as 2, and X_d can be computed using the corrosion current density (i_{corr}) of 0.35 μA/cm^2 that was mentioned in Val's study [26].

On the other hand, the behavior of SFRC in tension is described by the relationship between load and crack mouth opening displacement (CMOD), as illustrated in Fig. 2(b). The tension softening curve based on tension fracture energy (G_f), as specified in the *fib* Model Code 2010 [27], is defined in the tension behavior of SFRC. In this case, the peak value of the tensile stress was assumed based on the tensile strength (f_t') calculated by the corresponding compressive strength of the damaged SFRC. After reaching the peak value, the drop of tensile strength is determined based on the softening branch of ordinary concrete, as considered by the nonlinear model of Hordijk et al. [28]. However, the post-peak behavior of this material was defined based on the stress-crack curve as a linear model. The linear post-cracking relationship is described by the serviceability residual strength (f_{Fts}) at point D and the ultimate residual strength (f_{Ftu}) at point E, as seen in Fig. 2(b).

3.2. Steel reinforcement modeling

The residual capacity of corroded steel reinforcement (i.e., strength and ductile behavior of reinforcement) is mainly affected by the section loss along its length [29]. Because the pitting corrosion is complicated to model, the corroded steel reinforcement can be modeled by reducing the cross-sectional area along its length as uniform corrosion. Fig. 3 presents a bilinear stress-strain model for non-corroded and corroded reinforcements. The mechanical behavior of steel reinforcement is characterized by the yield tensile strength (f_y), ultimate tensile strength (f_u), and modulus of elasticity (E_s). Meanwhile, the deformation of steel reinforcement is represented by the strain values ε_y and ε_u at the yielding plateau and end failure.

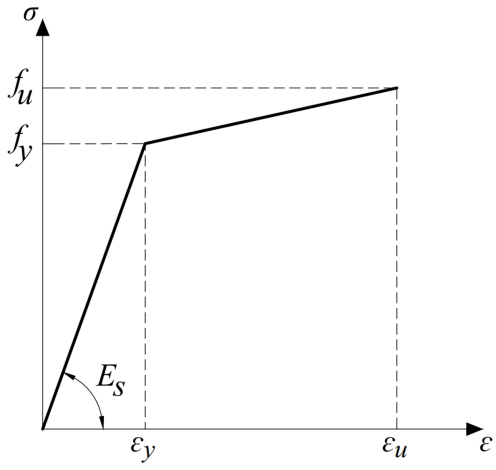

Figure 3. Steel constitutive model

3.3. Steel-SFRC interface modeling

Two major elements impacting the adhesive stress-sliding displacement relationship are the confined effect caused by stirrups in the RC structure and the mass loss of steel reinforcement after corrosion. The initial bond strength grew progressively when reinforcement corrosion developed but reduced considerably when corrosion cracks propagated. However, depending on how the concrete

cover is constructed and the number of steel rebars used, the bond loss between concrete and corroded reinforcement is often attributable to the degradation mechanism. The bond stress-slip diagram presented by Kallias and Rafiq [30] and Maaddawy et al. [31] is used to describe the bond deterioration between concrete and reinforcement. This study employs the bond stress-slip relationship in the *fib* Model Code 2010 [27] to simulate the good bond, as seen in Fig. 4.

In detail, the maximum bond strength ($\tau_{\max}$) can be computed by Eqs. (4) and (5). For the non-corroded beam, the maximum bond strength was 12.6 MPa, which was corresponding to the slip $s_1 = s_2 = 0.6$ mm, $s_3 = 2.5$ mm, and an exponential factor $\alpha = 0.4$. Meanwhile, to simulate the slipping failure of corroded beams with the unconfined effect, slip s_1 was set near s_2, and the bond stress started to sink after reaching the bond strength with the loss of concrete compressive strength. As shown in Fig. 4, the s_3 value drops as the bond stress (τ_f) approaches zero.

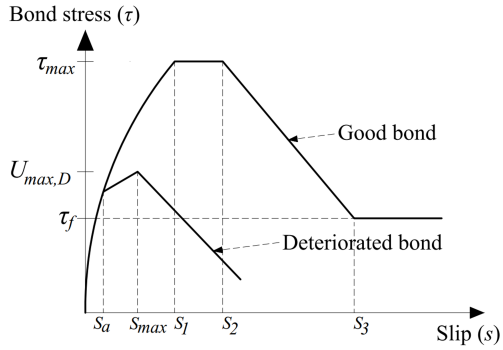

Figure 4. Steel-concrete interface constitutive model [30]

$$\text{For non-corroded beam:} \quad \tau_{\max} = 2.5\sqrt{f_c'} \tag{4}$$

$$\text{For corroded beam:} \quad \tau_{\max} = 1.25\sqrt{f_c'} \tag{5}$$

3.4. FEM validation

Fig. 5 illustrates the three-dimensional layout of the modeled beams. In this study, SFRC is modeled using isoparametric solid brick elements (CHX60) having 20-node with a regular mesh size of 25×25×25 mm. These elements feature three degrees of freedom per node x, y, and z and are based on quadratic interpolation and Gauss integration. In one direction, strain and stress change linearly, while they fluctuate quadratically in the other two directions. For properties of concrete, the compressive strength in the simulation was estimated using that as specified by the *fib* Model Code 2010 [27]. The tensile strength of deteriorated concrete due to corrosion was taken as 2.89 MPa in all circumstances in this study. Finally, the modulus of elasticity was computed based on the compressive strength, as indicated in Table 1. Besides, the steel rebars are modeled using three-node integrated truss elements (CL9TR) that allow representing bond-slip reinforcement. In the NLFE model of SFRC beams, the bond stress-slip relationship between steel rebars and concrete in non-corroded and corroded situations is modeled using the interface element.

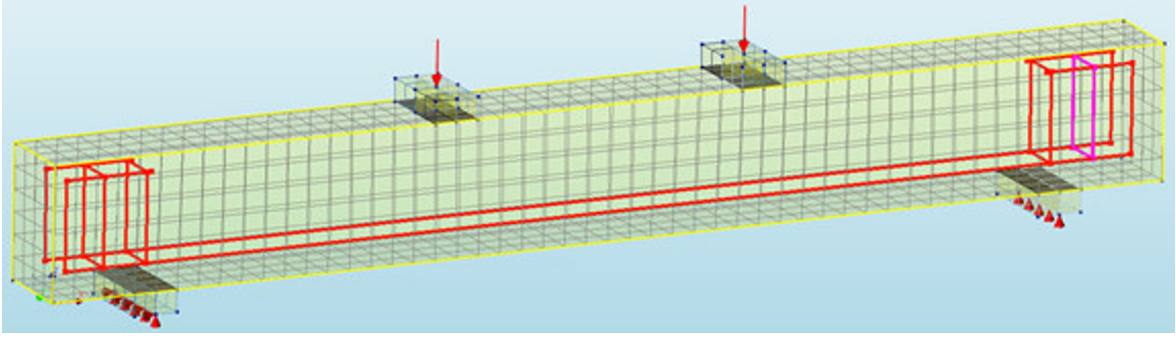

Figure 5. Three-dimensional model of SFRC beam specimens

Table 1. Material parameters used in the FEM

Parameter		Symbol	Beam specimens	
			BF-1.2	BC-1.2-7
Compressive strength of concrete (MPa)		f_c'	43.0	29.6
Tensile strength of concrete (MPa)		f_t'	3.52	2.89
Modulus of elasticity of concrete (GPa)		E_b	36	34
Compressive fracture energy (Nmm/mm^2)		G_c	22.48	18.95
Tensile fracture energy (Nmm/mm^2)		G_f	0.089	0.076
Yield tensile strength of steel rebars (MPa)	D10 (mm)	f_y	560	560
	D8 (mm)		534	534
Ultimate tensile strength of steel rebars (MPa)	D10 (mm)	f_u	652	652
	D8 (mm)		757	757
Modulus of elasticity of steel rebars (GPa)	D10 (mm)	E_s	200	200
	D8 (mm)		200	200
Reinforcement/concrete bond strength (MPa)		τ_{max}	12.6	5.4

Table 1 also includes the yield tensile strength and ultimate tensile strength of longitudinal reinforcements. The influence of steel corrosion was modeled numerically by reducing the cross-section of longitudinal reinforcement depending on the corrosion degree. For the non-corroded beam, the bond strength was calculated by the bond-slip curves, as illustrated in Fig. 4.

Two NLFE models for non-corroded and corroded SFRC beams were analyzed for FEM accuracy. Fig. 6 compares the tested and simulated results for the load-displacement at the middle span. Due to the position of the displacement measuring devices on the specimen, the initial stiffness between

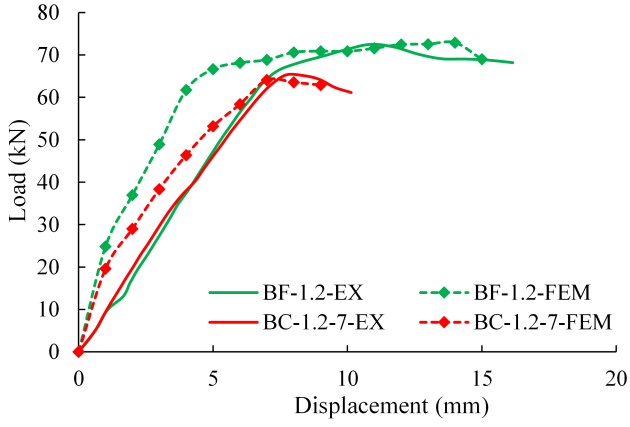

Figure 6. Load-deflection curves of beam specimens from the experiment and FEM

experimental and modeled beams in linear and nonlinear behaviors is different. The devices were installed on the bottom surface of the tested beam, while displacement points in FEM were determined at the loading point. Additionally, because of the stress locking in the smeared crack concrete model, the simulated stiffness after cracking was higher than that of the experiment [32, 33]. Table 2 compares the load-carrying capacity between the predicted and experimental data. The deviation between the maximum load obtained from the model ($P_{u,FEM}$) and experiment ($P_{u,EXP}$) is only 2 to 3% for the above non-corroded and corroded SFRC beams. That demonstrates a good agreement of model validation for the maximum load.

Table 2. Comparison between experimental and FEM results

Beam	Maximum load (kN)		Ratio $P_{u,EXP}/P_{u,FEM}$	Failure mode
	$P_{u,EXP}$	$P_{u,FEM}$		
BF-1.2	74.0	72.8	1.02	Flexure
BC-1.2-7	66.3	64.1	1.03	Shear and splitting

Moreover, FEM is used to describe the failure mechanism of experimental beams. As a result, Fig. 7 demonstrates the flexural failure in the SFRC control beam BF-1.2. The numerical results show

(a) Crack pattern at the failure

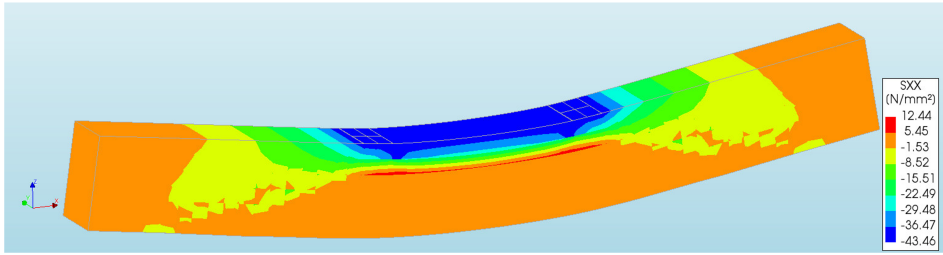

(b) Total Cauchy stress in concrete

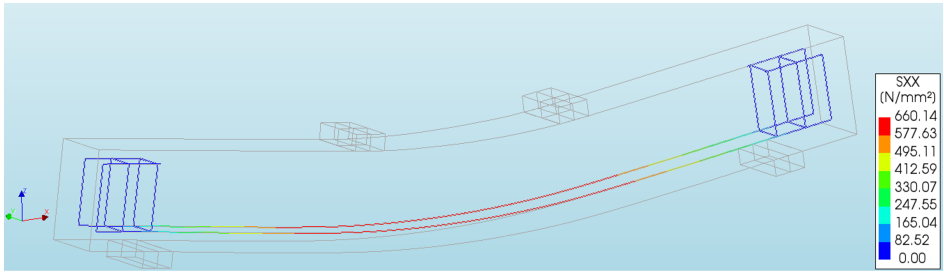

(c) Cauchy stress in steel reinforcement

Figure 7. Failure mode and stress distribution in the control beam

that the Cauchy stress obtained in the longitudinal reinforcement reaches beyond the yield tensile strength of 652 MPa, and the total Cauchy stress distributed on the concrete beam also exceeds the compressive strength of 43 MPa.

Fig. 8 shows the shear failure of the corroded beam in FEM compared to the experimental beam BC-1.2-7. Because of the tensile stress, inclined cracks in the corroded beam were propagated along the longitudinal rebars. However, the a/d ratio of this beam may be affected as a result of the load transfer mechanism from concrete to steel reinforcement. An inclined crack in FEM developed due to the quick fracture and sudden loss of loading capacity at 7 mm of mid-span displacement.

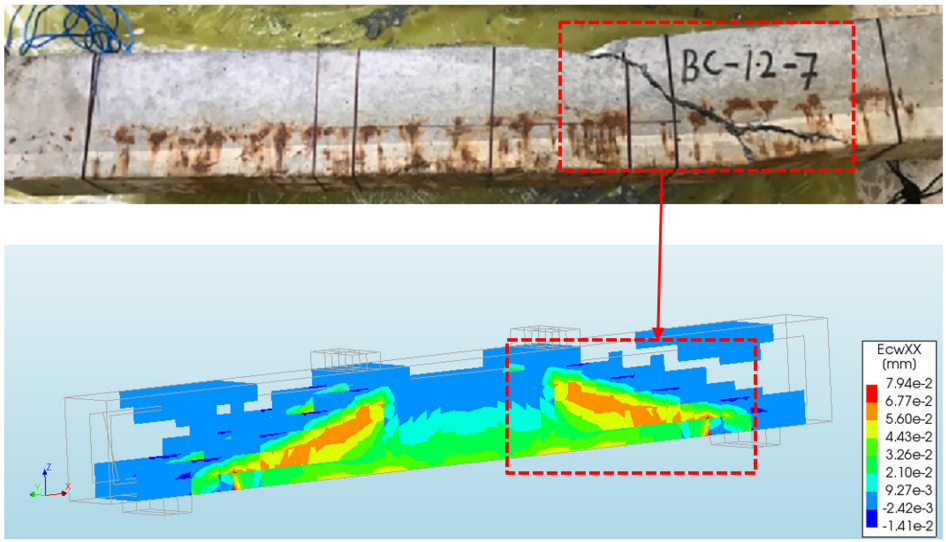

Figure 8. Cracking pattern of corroded SFRC beam by experiment and FEM

4. Parametric study

4.1. Effect of concrete compressive strength

In this study, three NLFE models have been made to investigate the effect of concrete compressive strength on corroded SFRC beam behavior. The modeled beams, denoted BC-1.2-7-B25, BC-1.2-7-B30, and BC-1.2-7-B35, have concrete compressive strengths of 25, 30, and 35 MPa. These compressive strengths are frequently used in designing and manufacturing RC components for practical works. The load-displacement curves with varying concrete compressive strengths are shown in Fig. 9. The average value generated from the predicted value is roughly 90% of that obtained in FEM.

As shown in Fig. 9, a decrease in the concrete compressive strength from 40 MPa to 35, 30, and 25 MPa reduces the maximum load of SFRC beams decreases by 10.7%, 14.5%, and 28.4%, respectively, corresponding to 57.2, 54.8, 45.9 kN compared to 64.1 kN on the modeled beam BC-1.2-7-FEM. The maximum load insignificant rises if the concrete compressive strength is 30 or 35 MPa. By contrast, the maximum load significantly increased as the concrete compressive strength increased from 25 to 40 MPa. This is because increasing the concrete compressive strength results in an increase in the initial stiffness of the beam. Before the failure, the displacement of the beam with higher concrete strength is smaller than that of the beam with a lower concrete strength at the same load level. Additionally, based on the load-displacement curves, it is possible to conclude that the failure mode remains unchanged when the concrete compressive strength ranges between 25 and 40 MPa.

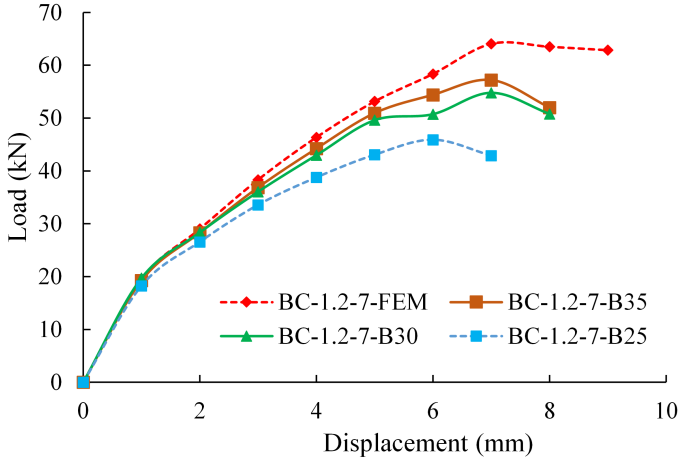

Figure 9. Load-displacement curves of corroded SFRC beams with different concrete compressive strengths

4.2. Effect of corrosion degree of longitudinal reinforcement

The corrosion degree of steel reinforcement should be a significant factor affecting the bearing capacity of beams. Therefore, four NLFE models were developed in this study to investigate the effect of steel reinforcement corrosion on SFRC beam behavior. These modeled beams denoted BC-1.2-10, BC-1.2-15, BC-1.2-25, and BC-1.2-30 represent the specimens with increasing corrosion degrees of longitudinal reinforcement of 10, 15, 25, and 30%, respectively. The results were obtained in FEM by considering the effect of steel reinforcement corrosion.

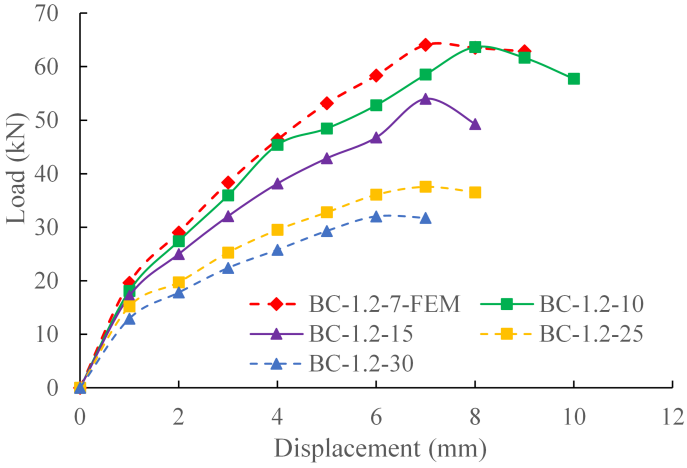

Figure 10. Load-displacement curves of modeled beams with varying corrosion degree

Fig. 10 shows load-displacement curves of beams with varying corrosion degrees. When the degree of reinforcement corrosion increased by 10%, 15%, 25%, and 30%, the concrete compressive strength reduced to 26.62, 22.81, 17.73, and 15.95 kN, respectively, according to Eq. (21). The results indicate that when the corrosion degree increased from 7% to 10%, the maximum load decreased marginally from 64.1 to 63.7 kN. Meanwhile, beam BC-1.2-7 failed at a 7 mm displacement, and

beam BC-1.2-10 failed at an 8 mm displacement. Because of that reason, the ductility of these beams increased. When the corrosion degree increased from 7% to 15%, 25%, and 30%, the maximum load dropped by 15.6%, 41.4%, and 50% (from 64.1 to 54.0, 37.6, and 32.0 kN, respectively). Moreover, the stiffness of the beam was also reduced. For 10% and 15% corrosion degrees, beams BC-1.2-10 and BC-1.2-15 remained in the same failure mode. However, when the corrosion degree increased by 25% and 30%, beams BC-1.2-25 and BC-1.2-30 fractured by crushing concrete in the compression zone, as illustrated in Fig. 11. Additionally, the concrete compressive strength decreases to 17.73 and 15.95 kN when reinforcement corrosion degrees are estimated to be 25% and 30%, respectively.

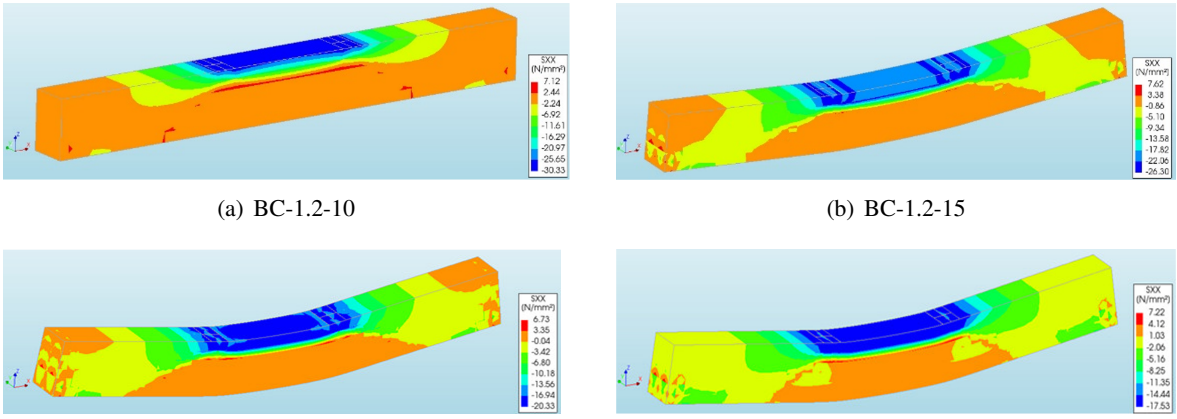

(a) BC-1.2-10 (b) BC-1.2-15

(c) BC-1.2-25 (d) BC-1.2-30

Figure 11. Concrete compressive stress distribution in modeled beams with different corrosion degrees

4.3. Effect of span-to-effective depth ratio

The shear span-to-effective depth (a/d) ratio illustrates the geometric theory of the shear resistant mechanism of beams. It is one of the significant parameters for the shear behavior of RC beams. Three NLFE models with variable a/d ratios were made to investigate the effect of a/d ratio on corroded SFRC beam shear behavior. These modeled beams denoted BC-1.2-7-2, BC-1.2-7-2.4, and BC-1.2-7-3.2 are presented as specimens having a/d values of 2, 2.4, and 3.2, respectively. The configuration of these specimens is presented in Fig. 12.

Fig. 13 demonstrates the load-displacement curves obtained in FEM with varying a/d ratios, respectively. When an a/d ratio was reduced from 2.8 on beam BC-1.2-7-FEM to 2.0, the maximum load raised from 64.1 to 73.2 kN corresponding to an increase of 14.3%. Furthermore, the initial stiffness of beam BC-1.2-7-2 is significantly improved compared to the other specimens. Meanwhile, if the a/d ratio equals 2.4, the maximum load decreased slightly from 64.1 to 60.8 kN corresponding to a 5.1% reduction, but the ductility decreased significantly. Likewise, the maximum load decreased from 64.1 to 57.4 kN for a 3.2 a/d ratio, corresponding to a 10.4% reduction. Thus, the results show that the effect of the shear span-to-depth ratio on the SFRC beam shear strength is smaller than that of concrete compressive strength. When a/d ratios range from 2.0 to 3.2, the load-carrying capacity of corroded SFRC beams with a 7% degree corrosion is reduced by approximately 22%.

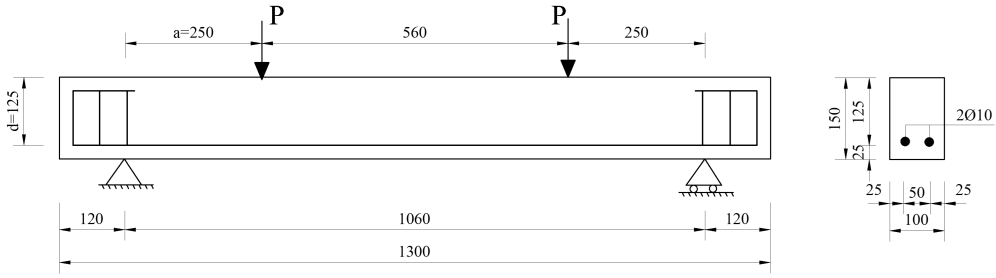

(a) BC-1.2-7-2

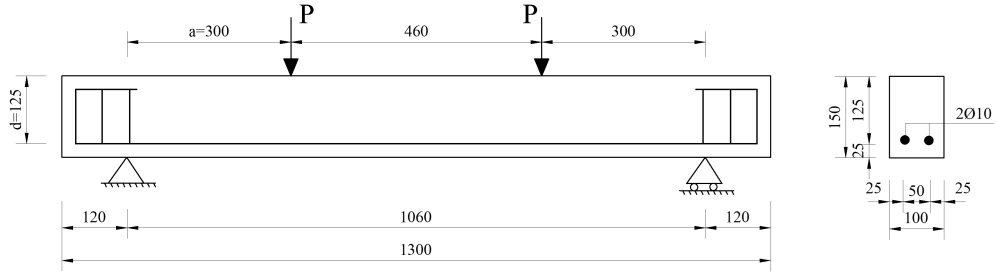

(b) BC-1.2-7-2.4

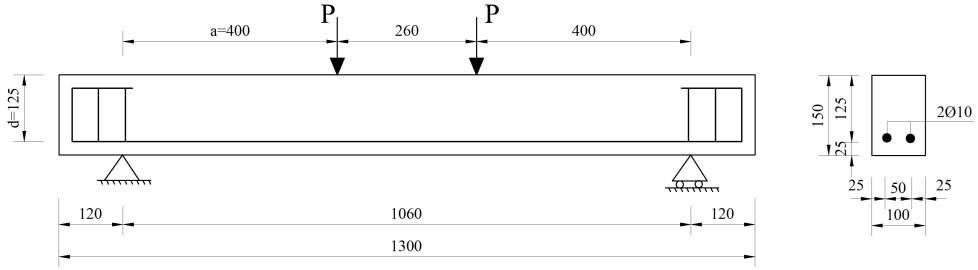

(c) BC-1.2-7-3.2

Figure 12. Configuration of modeled beams with different a/d ratios

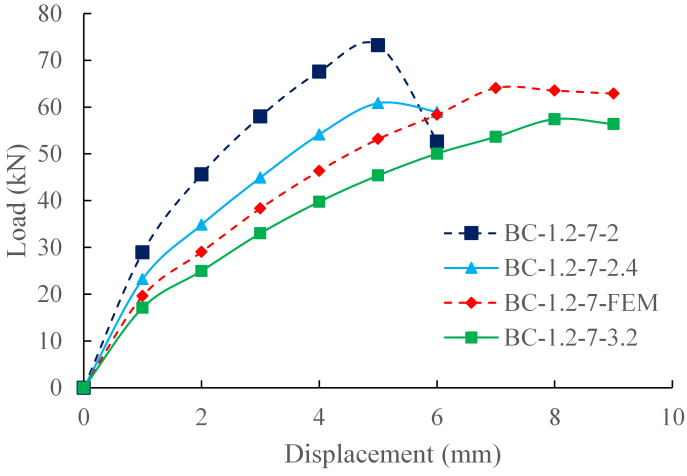

Figure 13. Load-displacement curves of modeled beams with different a/d ratios

4.4. Effect of steel reinforcement ratio

In order to investigate the influence of the steel reinforcement ratio, four NLFE models with variable longitudinal rebar diameters were built and discussed. These modeled beams denoted BC-1.2-7-D12, BC-1.2-7-D14, BC-1.2-7-D16, and BC-1.2-7-D18 are specimens with longitudinal rebars of D12, D14, D16, and D18 mm diameters, respectively.

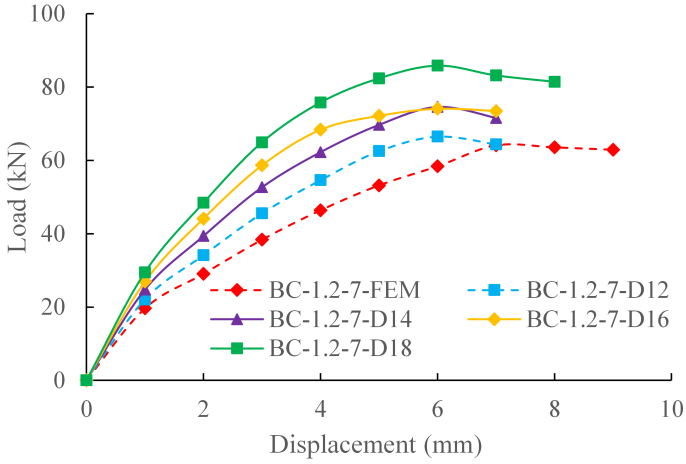

Figure 14. Load-displacement curves of modeled beams with different reinforcement ratios

Fig. 14 shows the load-displacement curves of modeled beams, while Fig. 15 illustrates the stress distribution of longitudinal rebars in FEM. As the reinforcement ratio raised by increasing the rebar diameter from 10 to 12, 14, 16, and 18, the stiffness of the beam improved dramatically as the maximum load increased from 64.1 to 66.5, 74.6, 74.1, and 85.8 kN, respectively. It shows that the maximum load increased by 3.8%, 16.4%, 15.6%, and 33.9%. However, with a slight increase in the reinforcement ratio (i.e., from D10 to D12 mm, or from D14 to D16 mm), the stiffness of SFRC beams increased while the maximum load remained relatively constant.

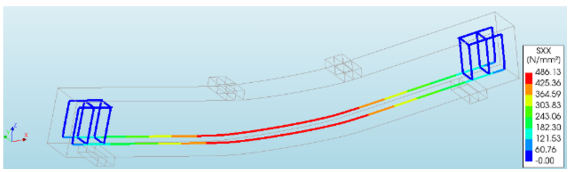

(a) BC-1.2-7-D12

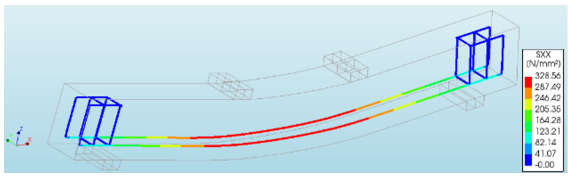

(b) BC-1.2-7-D14

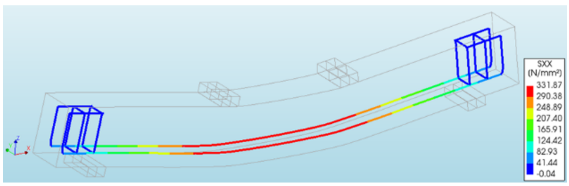

(c) BC-1.2-7-D16

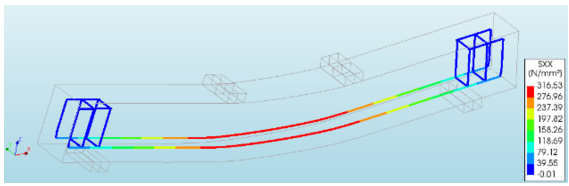

(d) BC-1.2-7-D18

Figure 15. Tensile stress distribution of steel reinforcement in modeled beams

5. Conclusions

This paper focused on the shear strength of SFRC beams with low corrosion of longitudinal reinforcement and without shear reinforcement. First, the NLFE models were built and verified to assess the shear behavior of non-corroded and corroded SFRC beams. The good agreement matched experimental data in terms of load-displacement curves, crack patterns, and failure modes. Then, a parametric study was conducted to investigate the effect of the main design-oriented parameters. The main conclusions may be derived as follows:

- For corroded SFRC beams, the FEM model can adequately describe the effect of steel fibers based on the load-CMOD relationship under corrosion attack. Apart from closely fitting the experimental value for the maximum load, FEM may be used to predict the shear behavior of corroded SFRC beams by considering the load-displacement curves, crack pattern, and failure modes.

- The shear strength of corroded SFRC beams raises as the concrete compressive strength increases, while a change in the reinforcement ratio could have a negligible effect. Particularly, the shear strength may remain proportional to the square root of the concrete compressive strength, including the effect of steel corrosion. For the remaining reinforcement ratio used, the shear strength of corroded SFRC beams decreases from 15.7 to 50% as the corrosion degree increases from 15 to 30%.

- The effect of the shear span-to-depth ratio on the SFRC beam's shear strength is smaller than that of concrete compressive strength. When a/d ratios increase from 2.0 to 3.2, the load-carrying capacity of corroded SFRC beams with a 7% degree corrosion is reduced by approximately 22%.

References

[1] Lim, S., Akiyama, M., Frangopol, D. M. (2016). Assessment of the structural performance of corrosion-affected RC members based on experimental study and probabilistic modeling. *Engineering Structures*, 127:189–205.

[2] Soltani, M., Safiey, A., Brennan, A. (2019). A state-of-the-art review of bending and shear behaviors of corrosion-damaged reinforced concrete beams. *ACI Structural Journal*, 116(3).

[3] Tan, N. N., Nguyen, N. D. (2019). An experimental study on flexural behavior of corroded reinforced concrete beams using electrochemical accelerated corrosion method. *Journal of Science and Technology in Civil Engineering (STCE) - HUCE*, 13(1):1–11.

[4] Nguyen, N. D., Tan, N. N. (2019). Prediction of residual carrying capacity of RC column subjected inplane axial load considering corroded longitudinal steel bars. *Journal of Science and Technology in Civil Engineering (STCE) - HUCE*, 13(2V):53–62. (in Vietnamese).

[5] Słowik, M. (2014). Shear failure mechanism in concrete beams. *Procedia Materials Science*, 3:1977–1982.

[6] Huang, L., Ye, H., Jin, X., Jin, N., Xu, Z. (2020). Corrosion-induced shear performance degradation of reinforced concrete beams. *Construction and Building Materials*, 248:118668.

[7] Nasser, H., Vrijdaghs, R., Van Steen, C., Vandewalle, L., Verstrynge, E. (2021). Effect of corrosion damage on the tension-stiffening effect: A numerical investigation of the RC tension bar. In *Proc. of the 2nd CACRCS Workshop Capacity Asssessment of Corroded Reinforced Concrete Structures*, 163–170.

[8] Tan, N. N., Kien, N. T. (2021). An experimental study on the shear capacity of corroded reinforced concrete beams without shear reinforcement. *Journal of Science and Technology in Civil Engineering (STCE) - HUCE*, 15(1):55–66.

[9] Tan, N. N., Nguyen, N. D. (2019). An experimental study on flexural behavior of corroded reinforced concrete beams using electrochemical accelerated corrosion method. *Journal of Science and Technology in Civil Engineering (STCE) - HUCE*, 13(1):1–11.

[10] Tan, N. N., Kien, N. T. (2020). Modeling the flexural behavior of corroded reinforced concrete beams with considering stirrups corrosion. *Journal of Science and Technology in Civil Engineering (STCE) - HUCE*, 14(3):26–39.

[11] Nguyen, T. K., Nguyen, N. T. (2021). Finite element investigation of the shear performance of corroded RC deep beams without shear reinforcement. *Case Studies in Construction Materials*, 15:e00757.
[12] Darwin, D., Dolan, C. W., Nilson, A. H. (2016). *Design of concrete structures*, volume 2. McGraw-Hill Education New York, NY, USA.
[13] Kim, H.-G., Jeong, C.-Y., Kim, M.-J., Lee, Y.-J., Park, J.-H., Kim, K.-H. (2017). Prediction of shear strength of reinforced concrete beams without shear reinforcement considering bond action of longitudinal reinforcements. *Advances in Structural Engineering*, 21(1):30–45.
[14] Lim, W.-Y., Hong, S.-G. (2016). Shear tests for ultra-high performance fiber reinforced concrete (UHPFRC) beams with shear reinforcement. *International Journal of Concrete Structures and Materials*, 10 (2):177–188.
[15] ACI 544.1 R-96 (2009). *State-of-the-art report on fiber reinforced concrete*. American Concrete Institute, Farmington Hills, MI, USA.
[16] Nguyen, N. T., Bui, T.-T., Bui, Q.-B. (2022). Fiber reinforced concrete for slabs without steel rebar reinforcement: Assessing the feasibility for 3D-printed individual houses. *Case Studies in Construction Materials*, 16:e00950.
[17] Bui, T. T., Nana, W. S. A., Doucet-Ferru, B., Bennani, A., Lequay, H., Limam, A. (2020). Shear performance of steel fiber reinforced concrete beams without stirrups: Experimental investigation. *International Journal of Civil Engineering*, 18(8):865–881.
[18] Torres, J. A., Lantsoght, E. O. L. (2019). Influence of fiber content on shear capacity of steel fiber-reinforced concrete beams. *Fibers*, 7(12):102.
[19] Keshtegar, B., Bagheri, M., Yaseen, Z. M. (2019). Shear strength of steel fiber-unconfined reinforced concrete beam simulation: Application of novel intelligent model. *Composite Structures*, 212:230–242.
[20] Taqi, F. Y., Mashrei, M. A., Oleiwi, H. M. (2021). Experimental study on the effect of corrosion on shear strength of fibre-reinforced concrete beams. *Structures*, 33:2317–2333.
[21] Ferreira, J., Manie, D. (2020). *DIANA Documentation release 10.4*, diana fea bv, netherlands edition.
[22] Nakamura, H., Higai, T. (2001). Compressive fracture energy and fracture zone length of concrete. In *Modeling of inelastic behavior of RC structures under seismic loads, ASCE*, 471–487.
[23] Nakamura, H., Nanri, T., Miura, T., Roy, S. (2018). Experimental investigation of compressive strength and compressive fracture energy of longitudinally cracked concrete. *Cement and Concrete Composites*, 93:1–18.
[24] Cape, M. (1999). Residual service-life assessment of existing R/C structures. Master's thesis, Chalmers University of Technology, Sweden and Milan University of Technology, Italy.
[25] Molina, F. J., Alonso, C., Andrade, C. (1993). Cover cracking as a function of rebar corrosion: Part 2—Numerical model. *Materials and Structures*, 26(9):532–548.
[26] Val, D. V. (2007). Deterioration of strength of RC beams due to corrosion and its influence on beam reliability. *Journal of Structural Engineering*, 133(9):1297–1306.
[27] fib Model Code (2010). *Fib model code for concrete structures 2010*. fib, Berlin, Germany.
[28] Cornelissen, H., Hordijk, D., Reinhardt, H. (1986). Experimental determination of crack softening characteristics of normalweight and lightweight. *Heron*, 31(2):45–46.
[29] Du, Y. G., Clark, L. A., Chan, A. H. C. (2005). Residual capacity of corroded reinforcing bars. *Magazine of Concrete Research*, 57(3):135–147.
[30] Kallias, A. N., Rafiq, M. I. (2010). Finite element investigation of the structural response of corroded RC beams. *Engineering Structures*, 32(9):2984–2994.
[31] Maaddawy, T. E., Soudki, K., Topper, T. (2005). Analytical model to predict nonlinear flexural behavior of corroded reinforced concrete beams. *ACI Structural Journal*, 102(4):550–559.
[32] Rots, J. G. (1991). Smeared and discrete representations of localized fracture. *International Journal of Fracture*, 51(1):45–59.
[33] Lakusic, S. (2019). Comparative study of various smeared crack models for concrete dams. *Journal of the Croatian Association of Civil Engineers*, 71(4):305–318.